Journal of Manufacturing Processes 16 (2014) 200–211

Contents lists available at ScienceDirect

Journal of Manufacturing Processes

journal homepage: www.elsevier.com/locate/manpro

Technical Paper

Influence of welding speed and power on residual stress during gas tungsten arc welding (GTAW) of thin sections with constant heat input: A study using numerical simulation and experimental validation

A. Ravisankar, Satish Kumar Velaga, Gaurav Rajput, S. Venugopal *

Indira Gandhi Centre for Atomic Research, Department of Atomic Energy, Kalpakkam 603102, Tamil Nadu, India

ARTICLE INFO

Article history:
Received 30 July 2013
Received in revised form 26 October 2013
Accepted 13 November 2013
Available online 31 January 2014

Keywords:
Numerical simulation
Heat source fitting
Weld pool size
Temperature distribution
GTAW
Residual stresses

ABSTRACT

The temperature distribution and residual stresses for a GTAW circumferential butt joint of AISI 304 stainless steel using numerical simulation have been evaluated. For evaluation of weld induced residual stresses, the analysis of heat source fitting was carried out with heat inputs ranging from 200 to 500 J/mm to arrive at optimal heat input for obtaining proper weld penetration and heat affected zone (HAZ). For this chosen heat input, the influence of different weld speeds and powers on the temperature distribution and the residual stresses is studied. The heat source analysis revealed the best choice of heat input as 300 J/mm. The residual stresses on the inner and outer surfaces, and along the radial direction were computed. Increase in temperature distribution as well as longitudinal and circumferential residual stresses was observed with the increase in weld speed and power. The validity of the results obtained from numerical simulation is demonstrated with full scale shop floor welding experiments.

1. Introduction

Gas tungsten arc welding (GTAW) is widely used to weld thin sections of stainless steel and non-ferrous metals such as aluminum, magnesium, and copper alloys. The circumferential butt joint is a common type of pipe joint in a variety of engineering applications such as oil and gas industries, nuclear, thermal power plants and chemical plants. The base metal and weld metal undergoes thermal cycles during the process of welding. These thermal cycles produce inhomogeneous plastic deformation, which results in the onset of the residual stresses in the weld metal. The presence of tensile residual stresses increases the susceptibility of the weld to fatigue damage, stress corrosion cracking (SCC) and fracture [1]. While manufacturing thin walled components these residual stress cause distortion of the component and make it difficult to control the dimensions of the components. Therefore, control of residual stresses and their distribution is important to avoid service failures and to ensure the dimensional compliance especially while welding thin walled sections. In order to control the residual stresses and their distribution a thorough understanding of the mechanism of development and the influence of welding parameters on the generation and distribution of residual stresses are required. The measurement of temperature distribution and residual stresses in the regions adjacent to the weld during and after the welding process is of prime importance for understanding the distribution of residual stresses and the influence of process parameters on the distribution of residual stresses.

It is well known that industries in their urge to complete the fabrication to meet the production schedules resort to welding with higher speeds by giving more power inputs. The higher welding speed, higher power input and transient or unsteady state thermal behaviors are often encountered during welding of thin sections. In view of the above, modeling tools are often used for the estimation of temperature distribution and residual stresses in the regions adjacent to the weld during and after the welding process. Finite element (FE) analysis is a proven tool for accurate assessment of thermo-mechanical behavior in circumferentially joined thin-walled structures and is being used in the evaluation of thermal cycles and welding residual stresses [2]. A review of literature [2–20] reveals that a number of investigations have been undertaken by various authors through numerical analysis coupled with experimental validation to understand the residual stresses arising from the differential temperature distributions during welding. Thus, regions near the weld center are likely to undergo severe thermal cycles because of such high concentrated heat source,

* Corresponding author. Tel.: +91 4427487323; fax: +91 4427480356.
E-mail addresses: venu@igcar.gov.in, venusrini@hotmail.com (S. Venugopal).

1526-6125/$ – see front matter © 2013 The Society of Manufacturing Engineers. Published by Elsevier Ltd. All rights reserved.
http://dx.doi.org/10.1016/j.jmapro.2013.11.002

which in turn generates residual stresses in the weld metal in the longitudinal as well as circumferential directions. Malik et al. [2] have evaluated the residual stresses on the inner and outer surfaces of cylinder for varying welding speeds with different heat input per unit volume. The above investigations reveal that the welding speed and power have strong influence on the distribution of residual stresses. Chin-Hyung Lee et al. [3] have carried out three dimensional FE analysis to estimate the residual stresses in circumferential welds of steel pipes with inside radius to wall thickness ratio ranging from 10.0 to 100.0. They have also illustrated the variation in residual stresses at different circumferential locations and the effects of diameter on residual stress distributions. Shim Y. et al. [4] considered a ramp heat input and included the effect of moving arc in their analysis. They also investigated the effect of various ramp times and observed that 20% of the actual heat input time is the best ramp time. Liang Wang et al. [5] have investigated the effect of laser travel velocities with constant power and the laser powers with constant velocity on the distribution of residual stress during laser welding of thin wall plates. In this study net heat input during welding process was also varied. Spina et al. [6] evaluated the effect of welding speeds on the weld profiles and distortion of the components during laser welding of AA 5083 sheets using numerical simulations. This study revealed that as the welding speed reduced the net heat input increased and vice versa. Brickstad et al. [7] used FE model to study the variation in weld heat inputs and the variation in the through-thickness of the weld and heat affected zone on the axial and hoop stresses for austenitic stainless steel pipe welds. Kazuo Ogawa et al. [8] investigated the residual stress in penetration nozzles by considering different nominal heat inputs and weld speeds at constant weld power for different weld passes. Chaowen Li et al. [9] carried out three dimensional finite element analyses of temperatures and stresses for increasing weld speeds with constant power on different samples. The above study reveals that increase in weld speed at constant power, increases the net heat input. Kermanpur et al. [10] studied the effect of variation in net heat input for a GTAW circumferentially butt welded pipes. The study revealed that increasing the heat input resulted in a wider weld pool along with a higher maximum temperature in the HAZ. Wu et al. [11,12] used different levels of heat inputs with different welding currents by keeping welding speed and voltage as constant for two different arc welding processes (double sided and plasma) in the numerical simulation. They also carried out numerical analysis to predict the temperature field and weld pool shape as a function of welding speed with constant laser power and current. Gery et al. [13] investigated the effect of variable welding speeds and energy inputs on the transient temperature distribution, shape and boundaries of fusion zone and HAZ. Dean Deng et al. [14] examined the influences of heat input on the size of HAZ, welding residual stress and distortion during numerical simulation of electro slag welding process. Dean Deng et al. [15] performed four different cases of welding simulations with constant weld current, voltage and speed to clarify the influence of phase transformation on the residual stress and welding deformation. Farid Vakili-Tahami et al. [16] carried out welding simulations on T-shape filet welding of AISI 304 stainless steel plates by considering the constant weld current, voltage and speed (i.e. constant heat input). Long et al. [17] predicted the temperature variations, fusion zone and heat affected zone as well as longitudinal and transverse shrinkage, angular distortion and residual stress for various welding speeds and plate thicknesses. Díaz et al. [18] carried out the comparative analysis of TIG welding distortions between austenitic and duplex stainless steels by considering two different net heat inputs for both the stainless steels. Jiang et al. [19] studied the effect of different welding heat inputs and layer numbers on residual stresses and deformation in repair welds of stainless steel clad plate. Yanhong Tian et al. [20] investigated the effect of heat input and welding speed on the temperature field, especially on the shape and dimensions of the weld pool. It can be observed from the above survey of literature that only limited investigations had been undertaken to study the effect of different conditions of weld speeds and powers with constant heat input on the variation in temperature distributions and residual stresses. Further, the information on the variation in longitudinal and circumferential residual stresses along the radial distance from the outer surface as a function of different weld speeds and powers with constant heat input is not available in the open literature. The relationship between weld speed and power versus residual stress and their distributions at constant heat input are important for the optimization of process parameters for welding of thin walled sections for achieving close dimensional tolerances in the products. The above mentioned relationships can be established, through FE modeling and these FE models can be used for optimizing the weld parameters for obtaining sound welds.

The objective of the present investigation is to estimate the temperature as well as residual stress distribution based on FE simulation during welding of AISI type 304 stainless steel by GTAW process for the purpose of optimizing the welding parameters for circumferential butt joint of circular sections of thin walled centrifugal extractors (CE) used for nuclear fuel reprocessing applications. Since the CE handle HNO_3 and rotate at about 3000 rpm the welds need to possess adequate penetration and the heat affected zone (HAZ) has to be as small as possible. For this study, circumferential welding of cylindrical components of 2.5 mm thick AISI 304 SS by GTAW process has been considered. The 2-D line diagram with boundary conditions for FE modeling is shown in Fig. 1.

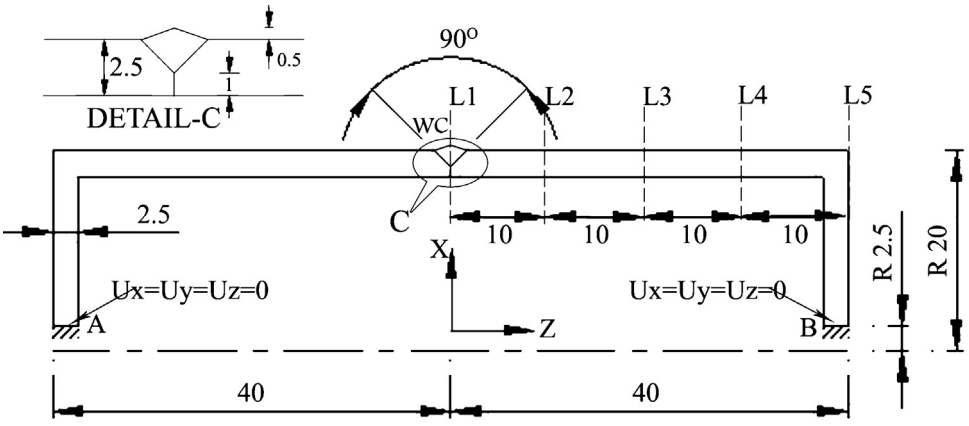

Fig. 1. Schematic 2-D line diagram of cylindrical work piece with boundary condition.

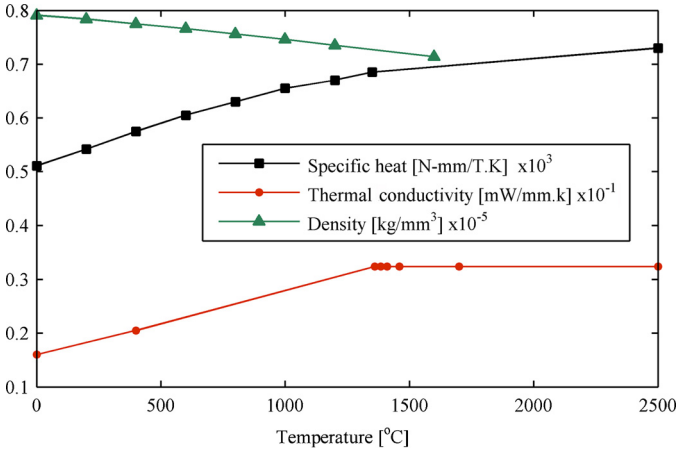

Fig. 2. Temperature dependent thermo-physical properties [16].

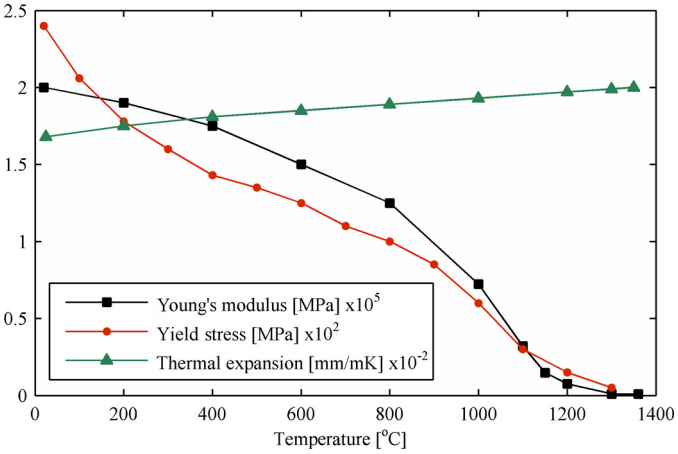

Fig. 3. Temperature dependent thermo-mechanical properties [16].

The appropriate heat input that gives the desirable weld penetration and heat affected zone (HAZ) has been arrived at based on the analysis of heat source fitting with different heat inputs ranging from 200 to 500 J/mm. The studies were undertaken at different welding speeds from 0.5 mm/s to 3 mm/s and at different power levels ranging from 150 W to 900 W at the appropriate heat input for evaluating the influence of power and welding speed on the temperature distribution and the residual stresses. The finite element analysis of single plane circumferentially butt joined cylinder is performed by using the commercial finite element package Sysweld®. The material properties of both base and the weld metal are assumed to be the same. Using Sysweld®, a detailed FE analysis was performed for the above mentioned welding speed and power levels to evaluate the temperature and the residual stresses distribution during circumferential butt welding of 2.5 mm thick × 40 mm diameter SS 304 cylindrical section. The results obtained from the FE simulation were validated experimentally by performing welding trials on 2.5 mm thick × 40 mm diameter SS 304 cylindrical sections.

2. Simulation of the weld process

2.1. Material properties

While performing the weld simulation, it is important to consider the variation of thermo-physical and thermo-mechanical properties of AISI 304 SS material with temperature. Thermo-physical properties such as thermal conductivity, specific heat capacity and density were considered. The thermo-mechanical properties that were taken in to account include Young's modulus, yield stress and coefficient of thermal expansion. The various properties of AISI 304 SS for the FE simulation were taken from ref [16] and the thermo-physical and thermo-mechanical properties are shown in Figs. 2 and 3 respectively. The solidus and liquidus temperatures were considered as 1360 °C and 1450 °C respectively and the value of latent heat of fusion is taken as 260 KJ/kg. The chemical composition of 304 SS used in the present investigation is given in Table 1 and the temperature independent material properties and constants such as Poisson's ratio, convection heat transfer coefficient, Stefan–Boltzmann constant and emissivity are listed in Table 2 [21]. The isotropic hardening model with linear strain hardening behavior was assumed for the FE analysis.

Table 1
Chemical composition (in wt%) of AISI 304 stainless steel.

C	Cr	Mn	Ni	Si	S	P	Fe
0.07	16–18	1.1–1.3	8.4–9.4	≤1	≤0.03	≤0.045	Rem

Table 2
Material properties used for FE simulation [21].

Property	Value
Poisson's ratio	0.33
Convection heat transfer coefficient	25 W/m^{2}K
Stefan-Boltzmann constant	5.670×10^{-8} W/m^{2}K^4
Emissivity	0.8

2.2. Finite element modeling

The thermal cycles and the evolution of the residual stresses are investigated by means of FE method using Sysweld®. In order to predict the temperature distribution and the residual stresses in a cylindrical object, a full 3-D model is developed by revolution of a 2-D mesh. The 2-D mesh and 3-D mesh are shown in Figs. 4(a) and (b), respectively. The details and dimensions of the components for simulation model are given in Fig. 1. The element type is

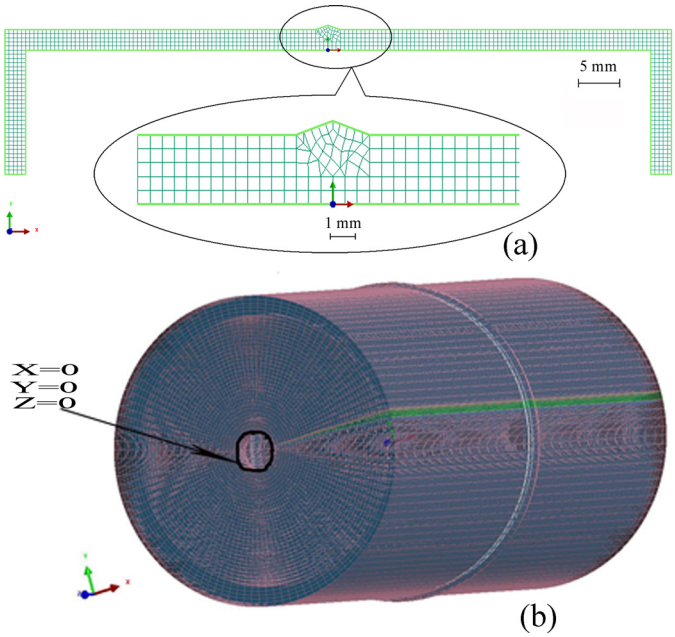

Fig. 4. Finite element mesh: (a) 2-D mesh and (b) 3-D mesh with boundary conditions.

Quard, 3-D solid with three translational degrees of freedom at each node. In longitudinal and radial direction, the element size was kept constant (i.e. 0.5 mm uniformly) including HAZ. In circumferential direction, the element size was also kept constant (i.e. 1 mm uniformly). The simulation procedure consists of two steps. In the first step, the temperature history was computed by the heat conduction analysis. In the second step, the temperature history in each node was employed as the thermal load for subsequent mechanical analysis. The thermal and mechanical models as well as heat source fitting are described in the following section.

2.2.1. Thermal model: temperature distribution

Generally, residual stresses are not only dependent on non-uniform temperature distribution generated during welding and but are also sensitive to transient temperature distributions due to moving heat source. In this study, the heat from the moving weld source is applied as a volumetric heat source with a semi ellipsoidal distribution as proposed by Goldak [22]. This is shown in Fig. 5 and can be expressed as

$$\dot{Q}\{x, y, z\} = \dot{Q}_0 \exp - \left\{ \frac{x^2}{a^2} + \frac{y^2}{b^2} + \frac{z^2}{c^2} \right\}, \quad (1)$$

where $\dot{Q}\{x, y, z\}$ represents the net internal volumetric rate of heat generation within the weldment, x, y and z are the coordinates in the semi ellipsoid reference system. In Fig. 5, a (i.e. a_f and a_r), b and c are the lengths which characterize the distribution of energy in heat source. The heat source is centered at the origin of a frame of reference which moves with the welding torch. The term $\dot{Q}_0$ is the power of the welding heat source and is defined as

$$\dot{Q}_o = \frac{2\eta VI}{abc\sqrt{\pi} erf\{z/c\}}, \quad (2)$$

where η, V and I are weld efficiency, voltage (volts) and current (amperes), respectively. Thereafter, the temperature distribution within the component is modeled by equation of conservation of energy and by non-linear isotropic Fourier heat flux constitutive equation.

In the present thermal model, mainly three factors such as heat losses due to radiation and convection, heat transfer in the weld pool and thermal effects during solidification have been considered. Radiation losses dominate at higher temperatures near to and in the weld zone while convection losses dominate at lower temperatures away from the weld zone. This thermal boundary condition is employed for all free boundaries of the cylindrical component. To consider the heat transfer due to fluid flow in the weld pool, a temperature dependent thermal conductivity was used. The thermal effects due to solidification of the weld pool were modeled by taking in to account the latent heat fusion. The ambient temperature was assumed to be 20 °C.

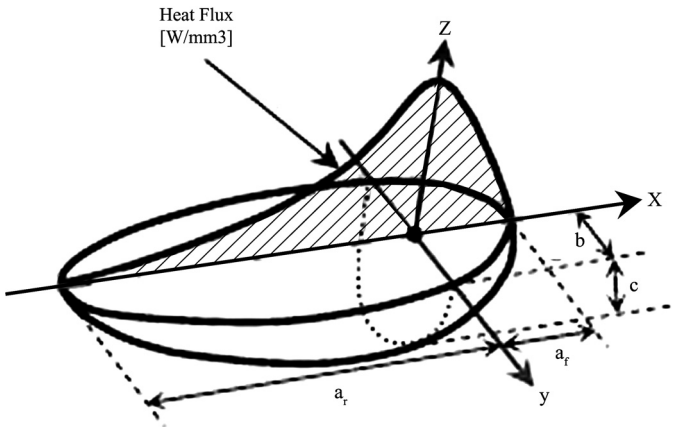

Fig. 5. Heat source model used in the present study.

2.2.2. Mechanical model: residual stresses

Analysis was carried out to evaluate the distortion and state-of-stress induced during welding. The same finite element model used in the thermal analysis was employed here. In order to prevent the rigid body motion, boundary conditions were used for mechanical analysis and these are shown in Figs. 1 and 4(b). With boundary conditions such as $U_X = U_Y = U_Z = 0$, the component is constrained at both ends in X, Y and Z directions. The mechanical analysis was conducted using the temperature histories that were obtained by the thermal analysis. The residual stresses arise due to incompatible strains caused by thermal gradients and microstructural changes, and therefore it is necessary to consider thermo-elasto-plastic formulation [23]. Hence, the total strain (ε) can be expressed as

$$\varepsilon = \varepsilon_e + \varepsilon_p + \varepsilon_{th} + \varepsilon_{tp}, \quad (3)$$

where ε_e is the elastic strain, ε_p is the plastic strain, ε_{th} is the thermo-metallurgical strain and ε_{tp} is that due to phase transformation. To calculate the thermo-metallurgical strain, the strains that arise due to thermal expansion and phase change were incorporated. This strain ε_{th} is given as

$$\varepsilon_{th} = \sum f_i \varepsilon_{th_i}(T), \quad (4)$$

where $\varepsilon_{th_i}(T)$ is the thermo-metallurgical strain corresponding to phase i at temperature T and f_i is the phase proportion of phase i. Though during welding it is known [9] that the solid state phase transformation can give rise to ε_{tp}, for the investigated AISI 304 stainless steel, the ε_{tp} component is negligible and is thus not considered.

The elastic strain component is computed knowing Young's modulus $E(T)$ and a constant Poisson's ratio ($\nu = 0.33$) for an isotropic material and the dependence of Young's modulus with temperature was used while evaluating the elastic strain. The plastic strain component due to large thermal gradients during heating and cooling was computed following the plastic model [23] which is for the case of isotropic hardening. The employed model further had the features of Von-Mises yield surface and temperature dependent mechanical properties.

2.3. Heat source fitting

The amount of heat from the welding process and subsequent cooling controls the weld penetration and the HAZ. The amount of heat input plays an important role because it affects the mechanical properties and metallurgical structure of the weld and HAZ. The heat input required for the welding mainly depends on the base metal thickness, its thermal conductivity and melting point of the base metal. In arc welding, energy is transferred from the welding electrode to the base metal by an electric arc. During welding, both the base metal and the filler metal are melted to create the weld. This melting is possible only if sufficient amount of power and energy density is supplied to the electrode. Heat input in GTAW is a measure of energy transferred per unit length of weld. The heat input (Q) in J/mm is the ratio of power and weld speed

$$Q = \frac{\eta VI}{S}, \quad (5)$$

where η = weld efficiency, V = voltage, I = current and S = welding speed (mm/min). In this investigation, four different cases of heat input were taken to study the distribution of molten zone and HAZ area. These four different cases are listed in Table 3. Temperature distribution for all cases of heat source fitting is shown in Fig. 6. For case-a, with 200 J/mm as heat input (Fig. 6a), improper weld

Table 3
Welding process parameters used for heat source fitting.

Case	Power = $V \times I$ (W)	Weld speed S (mm/s)	Heat input (J/mm)
a	200	1	200
b	300	1	300
c	400	1	400
d	500	1	500

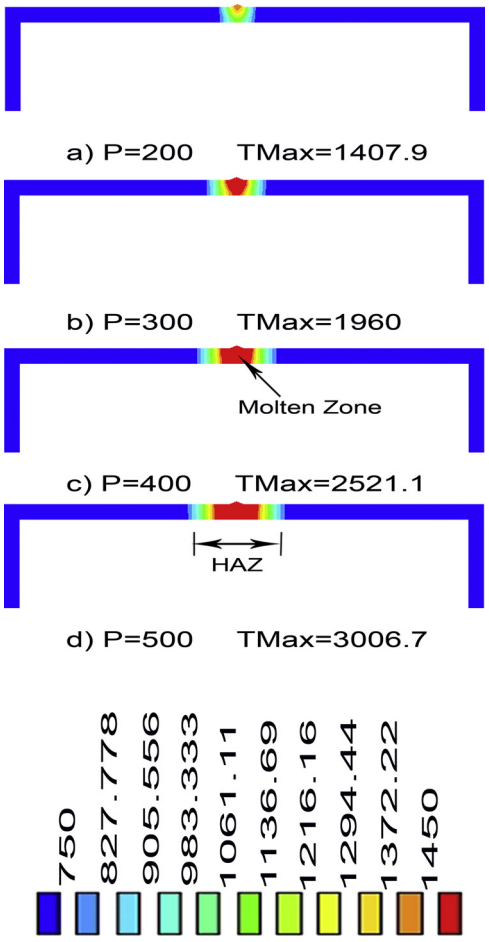

Fig. 6. Temperature distribution for different cases of heat source fitting.

Table 4
Heat source characteristic parameters.

Parameter	Value
Q_f (W/mm^3)	42.16
Q_r (W/mm^3)	42.16
a_f (mm)	1.2
a_r (mm)	1.2
b (mm)	1.2
c (mm)	1.15

Table 5
Summary of different combinations of weld speed and power.

Case	Weld speed S (mm/s)	Power = $V \times I$ (W)	Heat input (J/mm)
1	0.5	150	300
2	1	300	300
3	2	600	300
4	3	900	300

penetration and HAZ is observed since maximum temperature of 1407 °C was not sufficient for melting the base metal. For case-c and case-d (with 400 J/mm and 500 J/mm heat input), molten zone and HAZ are broadly spread. Maximum temperatures for case-c and case-d are noticed as 2521 °C and 3088 °C respectively, which may result in high welding distortions and residual stresses. Among the four cases, case-b (i.e. 300 J/mm heat input) was found to give better weld penetration with controlled molten zone and HAZ at the maximum temperature of 1960 °C. For this heat input (i.e. 300 J/mm), the Gaussian parameters for semi ellipsoid heat source as suggested by Goldak [22] are given in Table 4. The experimental weld pool shape and the predicted weld HAZ are shown in Fig. 7, and it could be seen that the results are in good agreement with each other. Further, the HAZ was found to be comprised of series of contours that ranged from 700 to 1450 °C (Fig. 7). The above observation directed us to study in detail the temperature distribution and the residual stresses for different combination of weld speed and power (Table 5) giving constant heat input of 300 J/mm. The results obtained based on simulation are discussed in the following section.

3. Results and discussions

3.1. Welding temperature characteristics (thermal analysis)

FE simulation of welding process, for the constant heat input of 300 J/mm at different combinations of weld speed and power, has been carried out for predicting the temperature characteristics at various locations away from weld. A typical result of the

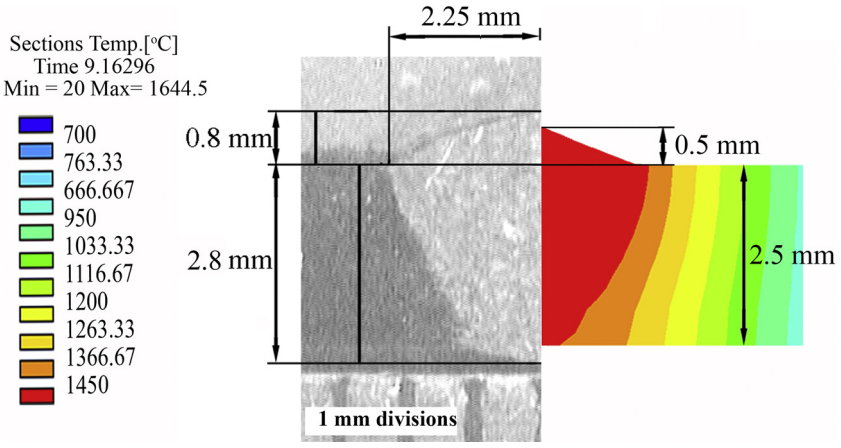

Fig. 7. The weld pool shapes obtained by experiments and FE simulation.

simulation is presented in Fig. 8, which depicts the three dimensional temperature profile on the outer surface at 65.8 s for the simulation condition mentioned in case-2 of Table 5. The elliptically shaped temperature distribution is observed on the external surface of the component and these are in agreement with the earlier results [2]. Figs. 9(a)–(e) depicts the temperature distribution on the outer surface during welding for five locations along the Z coordinate at 180° section (i.e. mid of the circumference) from weld start position. These five locations (L1–L5) are shown in Fig. 1. The temperature distribution profiles are shown in Fig. 9 for different combination of weld speed and power as mentioned in Table 5. As anticipated, peak temperatures are at the weld location (WL) as shown in Fig. 9a. From Figs. 9(a)–(e), it is apparent that peak temperatures are found to decrease with the measurement locations longitudinally away from the WL. The peak temperature and temperature distribution profile at each location are observed to be in good agreement with the welding process in practice [1–3]. It is clear that the temperatures at 180° section from the weld start position are high when heat source crosses the section. For instance, in case of Fig. 9(a) with the weld speed of 0.5 mm/s,

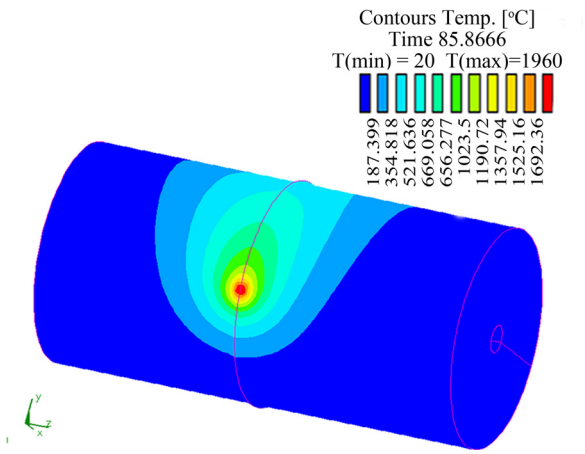

Fig. 8. 3-D temperature profile on the outer surface.

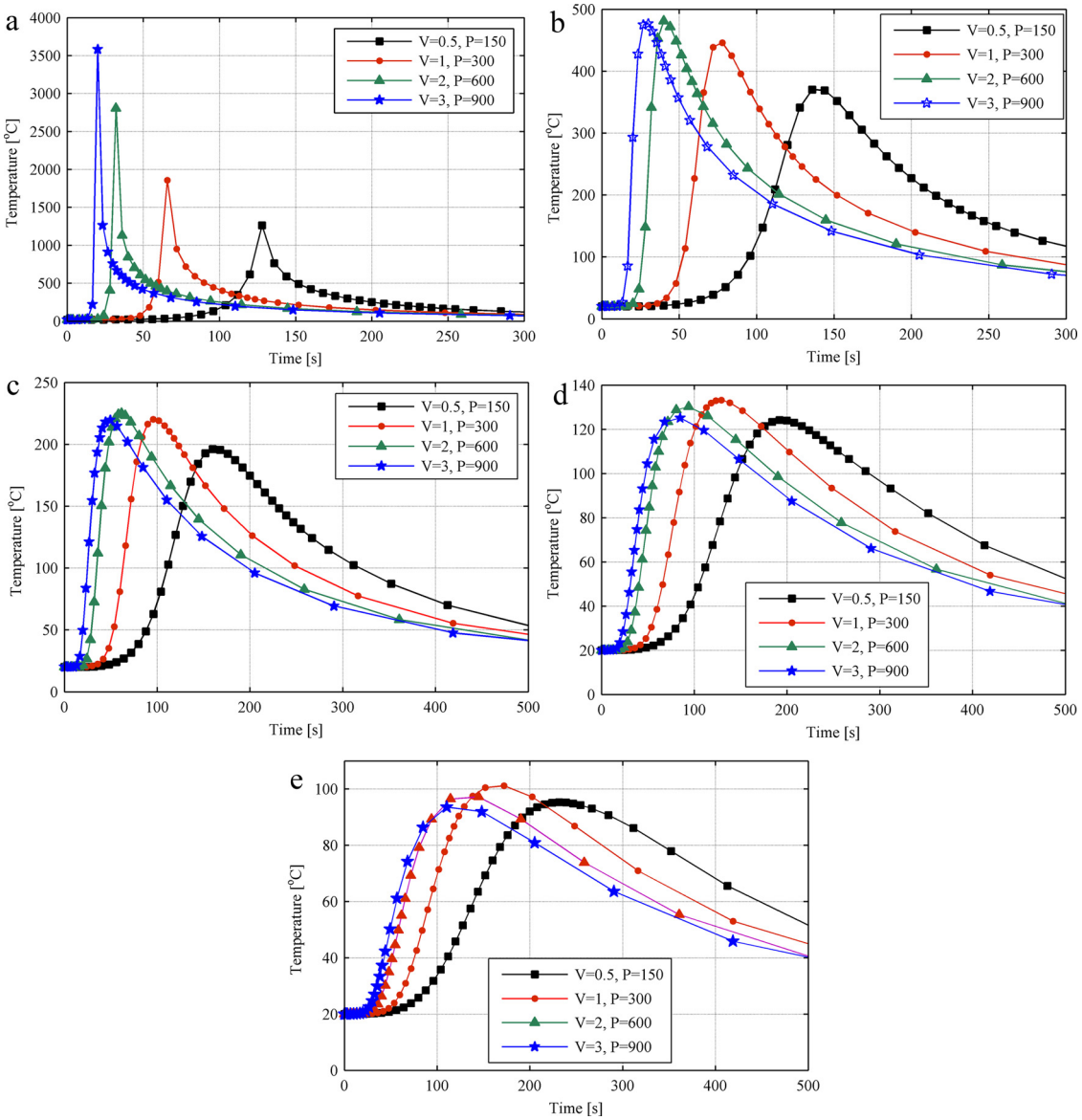

Fig. 9. Comparison between simulated transient thermal cycles for four different cases at different locations longitudinally away from weld center: (a) weld center, (b) 10 mm, (c) 20 mm, (d) 30 mm and (e) 40 mm.

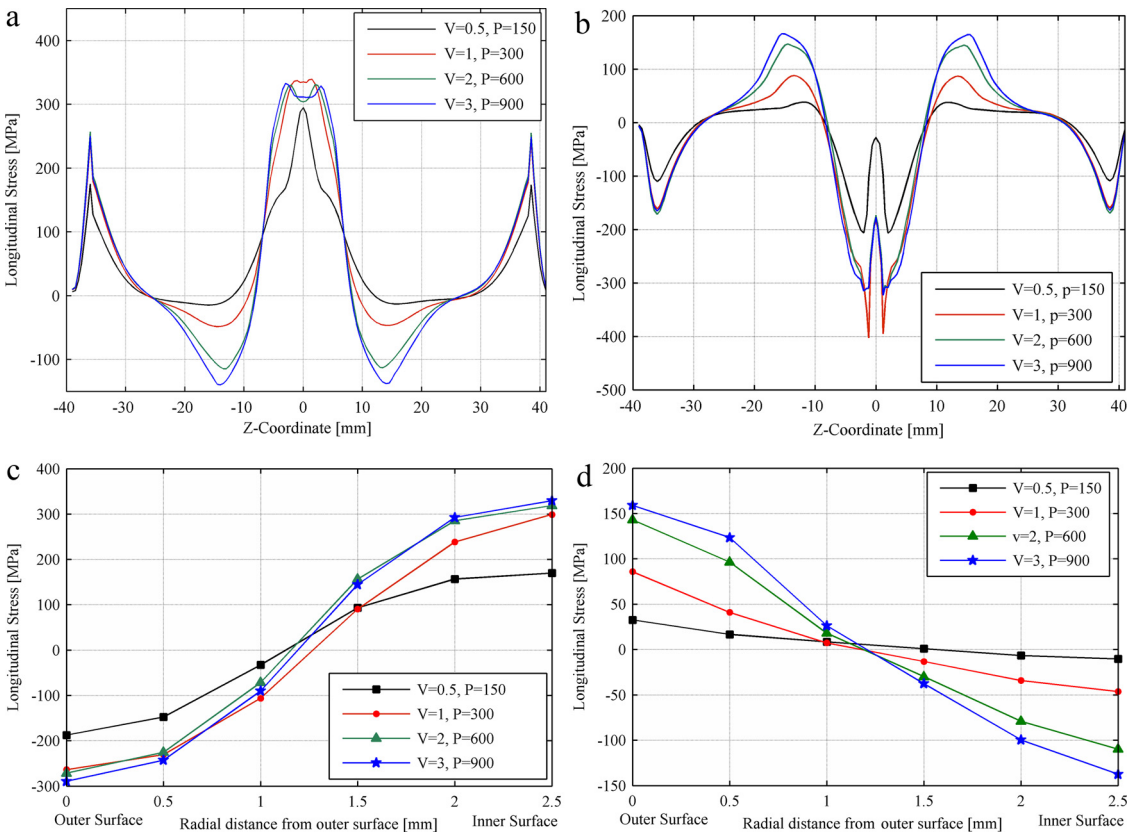

Fig. 10. Comparison between longitudinal residual stresses for different cases at 180° section from the weld start position: (a) on the inner surface, (b) on the outer surface, (c) along the radial direction from outer surface at 3 mm away from WC and (d) along the radial direction from outer surface at 14 mm away from WC.

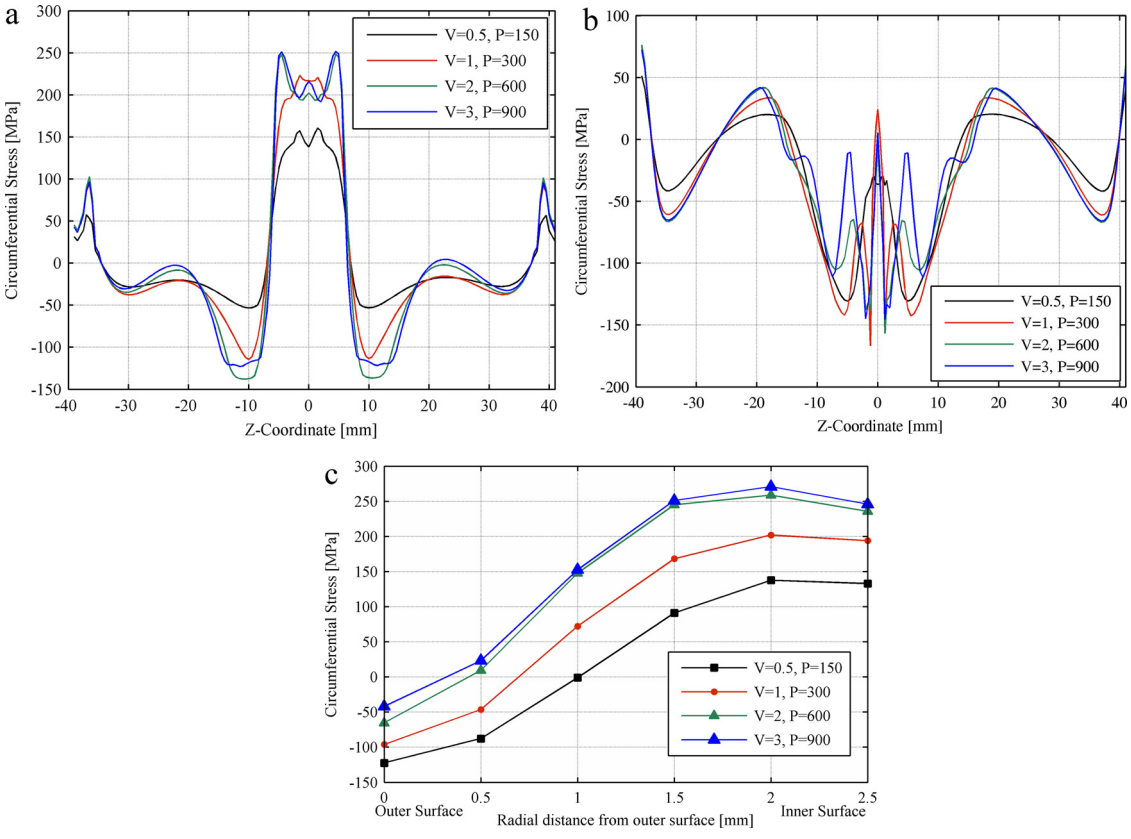

Fig. 11. Comparison between circumferential residual stresses for different cases at 180° section from the weld start position: (a) on the inner surface, (b) on the outer surface, (c) along the radial direction from outer surface at 4 mm away from WC.

when the weld torch travels around a circumference of $\pi \times D$ ($3.14 \times 40 = 125.6$ mm), the weld torch reaches the 180° section after 125.6 s. Hence, the peak temperature is observed at 125.6 s for 0.5 mm/s weld speed. Similarly, the peak temperature is observed at 62.8 s for 1 mm/s weld speed. Due to forward heat flow from the weld torch, a preheating action occurs and also the temperature falls slowly when the torch crosses the section.

3.1.1. Influence of weld speed and power on temperature distribution

The effect of the weld speed and power on the temperature distribution for various locations away from the weld is presented in Figs. 9(a)–(e). It is observed that the peak temperature increases at the weld center (WC) with increasing weld speed and power as shown in Fig. 9(a). It is discerning to note (Figs. 9(a)–(e)) that the difference in peak temperatures also gets reduced for the locations longitudinally away from the WL. The possible reason for such an observation could be that with an increase in the weld speed and power, the rate of heat input is higher than the rate of heat dissipation. This also would result in localized heating at the fusion zone.

3.2. Welding residual stress (mechanical analysis)

Based on the simulation, residual stresses in the longitudinal, circumferential and radial directions were obtained on the inner surface, outer surface and along the radial distance from the outer surface for varying weld speeds and powers with a constant heat input of 300 J/mm and are presented in Figs. 10–12, respectively. It is to be noted that these residual stress values correspond to 180° section from the weld start position as mentioned in Section 3.1. Detailed analysis has been carried out on the above results to understand the characteristics and the influence of varying weld speed and power on these residual stresses and these are discussed in the following sections.

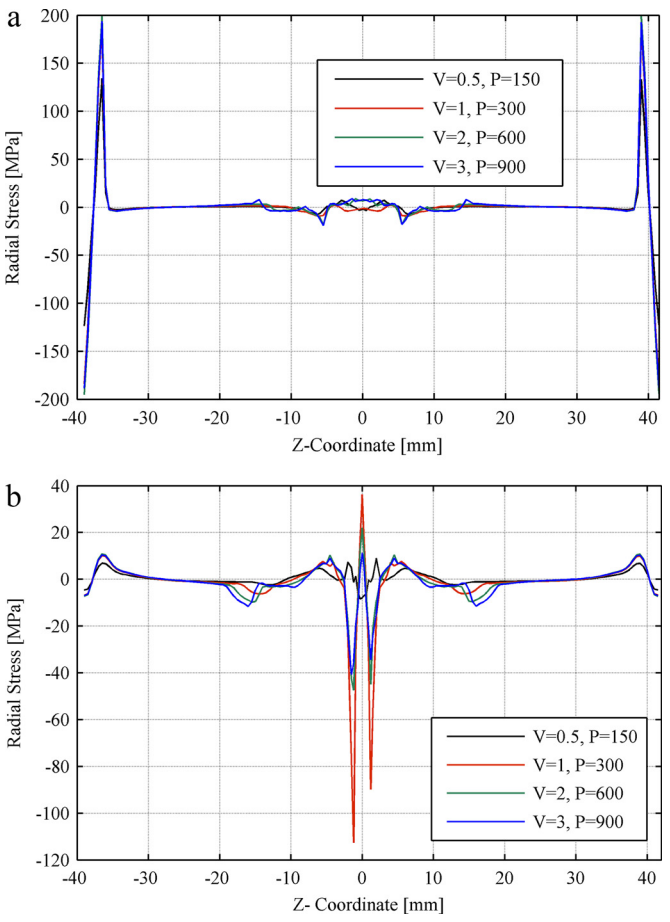

Fig. 12. Comparison between radial residual stresses for different cases at 180° section from the weld start position: (a) on the inner surface and (b) on the outer surface.

3.3. Longitudinal stress

The longitudinal stresses, normal to the direction in the circumferential joint of weld bead, are shown in Figs. 10(a)–(d). In these figures, the stress distribution was analyzed for the inner and outer surfaces, as well as the stresses along the radial direction from the outer surface at 3 mm and 14 mm away from the WC. It can be seen that the stresses were both tensile and compressive which arise due to temperature gradients, variable shrinkage patterns and the type of boundary condition imposed in this simulation work. Fig. 10(a) reveals that on the inner surface, the longitudinal tensile stresses show a peak at the WL and then decrease to compressive stresses. Further, stress reversal from compressive to tensile can be seen on both sides of the WC. The tensile to compressive reversal is found to occur at around 8 mm from the WC, whereas compressive to tensile at around 25 mm from the WC (Fig. 10(a)). On the other hand, the results on the outer surface show an opposite trend, i.e. compressive to tensile and then tensile to compressive. The transition from compressive to tensile was obtained at around 8 mm and that from tensile to compressive at around 34 mm on both sides of the WC (Fig. 10(b)). The observations and the trends seen on the inner and outer surfaces in this study were found to be in agreement with those obtained by other investigators [2,24,25]. It was also noticed (Figs. 10(a) and (b)) that the variation in the stress is maximum at the locations of 3 mm and 14 mm longitudinally away from the WC. The results corresponding to these locations are shown in Figs. 10(c) and (d), respectively.

3.3.1. Influence of weld speed and power

It can be seen in Fig. 10(a) and (b) that the stress values increase with increasing weld speed and power, irrespective of the locations along the Z coordinate. This increase in stresses for the location of 3 mm away from the WC was found to be significant with the increase in tensile stresses as 150 MPa on the inner surface, and that for compressive stresses as 100 MPa on the outer surface (Fig. 10(c)). Further, for the Z coordinate beyond 8 mm from the WC, the same increasing trend in compressive (Fig. 10(a)) and tensile stresses (Fig. 10(b)) was observed. It is noticed that peak tensile residual stresses occur within the fusion zone on the inner surface. At 3 mm longitudinally away from the WC, the magnitude of peak tensile residual stress is found to be 330 MPa, which is greater than the yield stress (i.e. 265 MPa) of the material. The presence of such high tensile residual stresses needs to be minimized, as they can cause fatigue damage, SCC leading to the material failure. Whereas on the outer surface, the peak tensile residual stresses were found to be lesser than the yield stress.

Figs. 10(a) and (b) reveal that the nature of residual stress, changes with respect to increasing Z coordinate. The results shown in Fig. 10(c) for 3 mm from the WC reveal that with increasing radial distance from the outer surface, the compressive stresses change over to tensile stresses at 1.25 mm. Whereas, it is interesting to note that for 14 mm as shown in Fig. 10(d) that the transition from tensile stresses to compressive occurs also at 1.25 mm distance radially from the outer surface (i.e. mid section between the outer and inner surfaces).

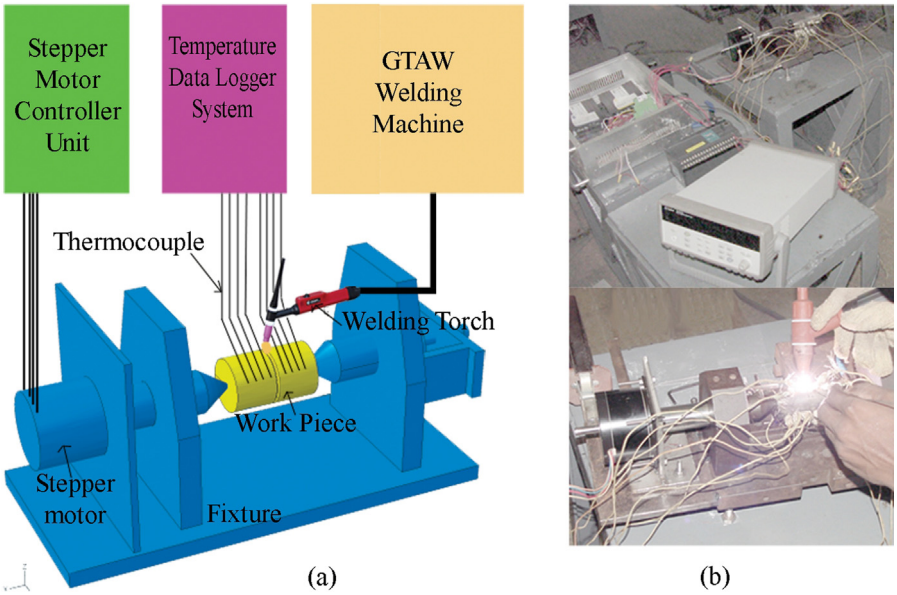

Fig. 13. Experimental setup used (a) schematic diagram and (b) welding setup with clamping fixture and data logging system.

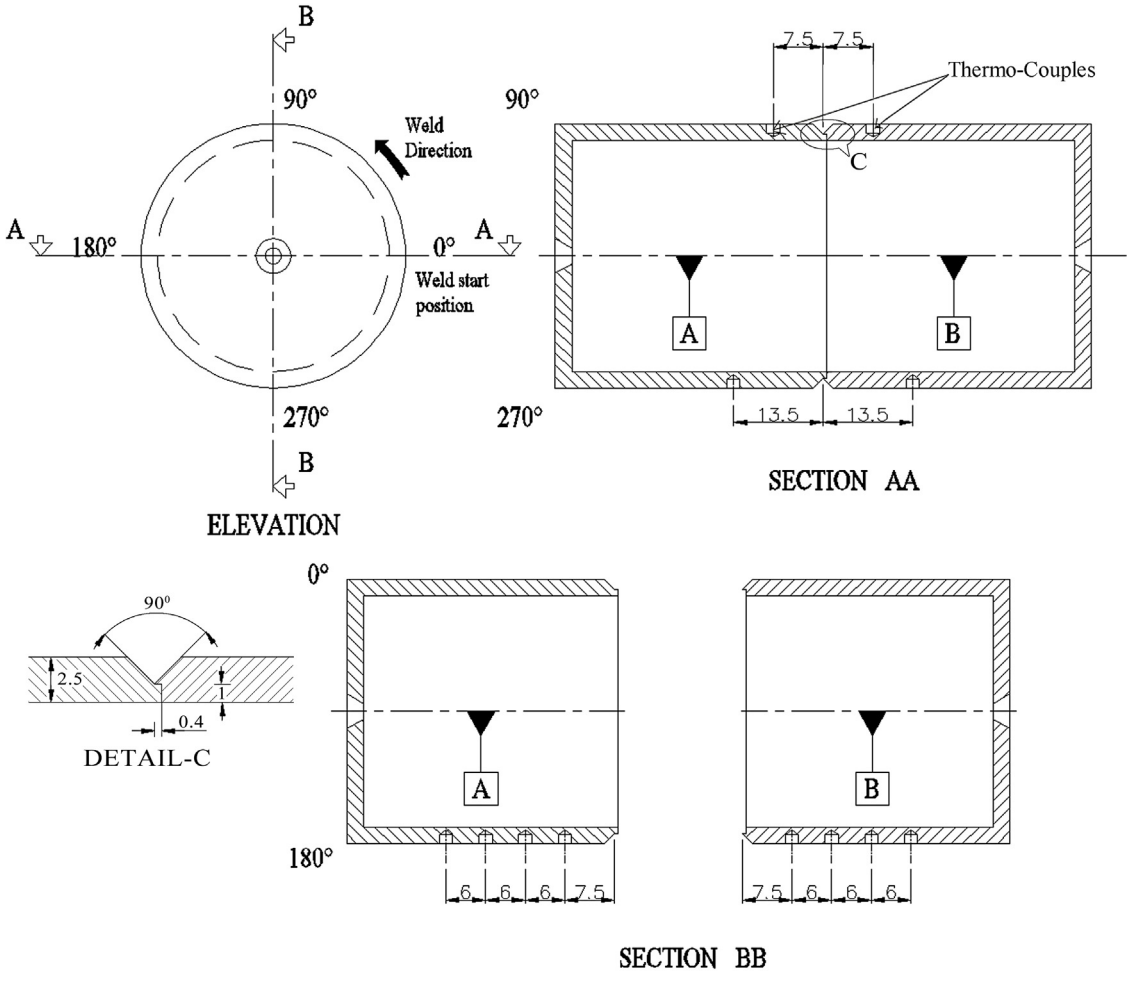

Fig. 14. Location of thermocouples and weld direction.

3.4. Circumferential stress

The expansion and contraction in the radial direction during thermal cycling can result in circumferential stresses that are along the direction of the weld. The analysis of the variation of circumferential stresses with *Z* coordinate and along the radial direction for various weld speed and power are described in Figs. 11(a)–(d). The results obtained on the inner (Fig. 11(a)) and outer (Fig. 11(b)) surfaces can be summarized as follows. While on the inner surface, the tensile residual stresses observed at the WL change over to compressive stresses, the reverse trend is observed for those on the outer surface. The transition in stress reversal was found to occur at 7 mm from the WC for the inner surface, whereas it was at 15 mm for the outer surface. The nature of compressive stress beyond 7 mm was wavy (Fig. 11(a)), whereas on the outer surface, it was zig-zag in pattern near HAZ (Fig. 11(b)). The characteristics of the circumferential stress along the radial direction for the location of 4 mm in the Z coordinate are shown in Fig. 11(c). The trends for circumferential stresses also concur well with the observations recorded by the previous researchers [2,24,25].

3.4.1. Influence of weld speed and power

It was observed that with an increase in the weld speed and power, the circumferential stress increased and this increase was found to be significant. For the location of 4 mm from the WC (Fig. 11(c)), the magnitude of increase in tensile residual stresses was ≈120 MPa on the inner surface, whereas it was ≈100 MPa for compressive stresses on the outer surface. It is important to notice that the peak tensile residual stress of ≈250 MPa observed could be reduced to ≈130 MPa by decreasing the weld speed (i.e. 0.5 mm/s) and power (i.e. 150 W) as shown in Fig. 11(c). This reduction in residual stress is much less than that of the yield stress (i.e. 265 MPa), which is beneficial to improve the service life of the component. The results on the circumferential residual stresses along the radial direction revealed that the transition from compressive to tensile stresses occurs at a distance between 0.5 and 1 mm radially from the outer surface as shown in Fig. 11(c).

3.5. Radial stress

The radial residual stresses on both sides of the WL are generated because of the variable shrinkage patterns. The variable shrinkage patterns are caused due to the temperature gradients across the wall thickness in the component during welding. The results of these radial stresses are presented in the following. Figs. 12(a) and (b) exhibit the radial stress distribution on the inner and outer surfaces, respectively and these are for 180° cross-section from the weld start position. An interesting observation to note is that unlike the longitudinal and circumferential stresses, the radial stresses were not influenced by the weld speed and power. It can also be seen that the stresses were negligible on both sides of the WL along the Z coordinate except at 40 mm distance on the inner surface (Fig. 12(a)) and at the WL on the outer surface (Fig. 12(b)). Further, it is evident that the nature of the stress was tensile (i.e. at 40 mm) on the inner surface, whereas it was tensile to compressive in the HAZ on the outer surface. The peak tensile stress observed at 40 mm along the *Z* coordinate (Fig. 12(a)) may be attributed to reasons such as boundary condition imposed during welding and the geometric configuration employed in this study. Based on the above observations, it can be concluded that the influence of weld parameters (i.e. investigated weld speed and power) can be ignored for the analysis of radial stress distribution.

Figs. 10(b), 11(b) and 12(b), correspond to the distribution of longitudinal, circumferential and radial residual stress on the outer surface. The important observation in above mentioned figures is that there are sharp points of stress reversal. The stress reversal takes place at the interface between molten zone and the adjoining region. The possible reason for this could be drastic change in physical and mechanical properties of molten material and the solid material.

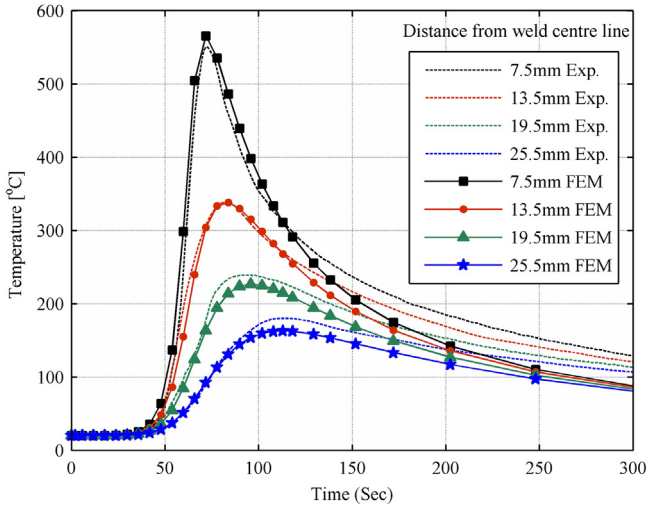

Fig. 15. Comparison of experimentally obtained temperature profiles with those from FE simulation for different locations.

4. Experimental validation

The results obtained from the numerical simulation were validated with experiments conducted using GTAW process with SS 308 as the filler material having diameter of 0.8 mm. The experiments were performed only at a particular weld speed of 1 mm/s with similar geometric dimensions as shown in Fig. 1. Figs. 13(a) and (b) shows the schematic of the experimental setup and the welding setup respectively. The welding setup was equipped with automated speed control through a stepper motor to maintain a constant weld speed of 1 mm/s. The two cylinders were initially joined by tack weld at four locations (each 90° apart). Temperature was measured using Chromel-Alumel (K-type) thermocouples connected at twelve locations at the outer surface by silver brazing. The weld start position, weld direction and the location of thermocouples are shown in Fig. 14. The thermocouples were located at 90°, 180° and 270° from the weld start position. The transient thermal cycles were recorded with the data acquisition system for time interval of 1 s. For welding, 37 A and 10 V were chosen to supply the heat input of about 300 J/mm as employed in the simulation. Following Eq. (5), it can be easily seen that these process parameters with process efficiency, $\eta = 0.8$ gives the heat input of 296 J/mm. It is important to emphasize that the experimental data presented correspond only to a particular heat input (i.e. case 2 in Table 5). The temperature profiles reported were for the 180° section (i.e. 8 locations) as shown as section 'BB' in Fig. 14 and the values are the average of those obtained on both sides of the WL. The transient temperature profiles obtained experimentally and their comparison with those from simulation for different locations are shown in Fig. 15. It could be observed that the experimental and simulated FE results match well at locations of 7.5 and 13.5 mm longitudinally away from the WC. Whereas, for 19.5 and 25.5 mm locations, the experimental values were marginally higher than that of the FE results. The maximum difference in peak temperatures between experimental and FE simulation was observed to be 9.4% at 25.5 mm location. The rate of increase in temperature also was in correspondence with each other. However, during cooling the experimental values were slightly higher than that of the FE results and this would

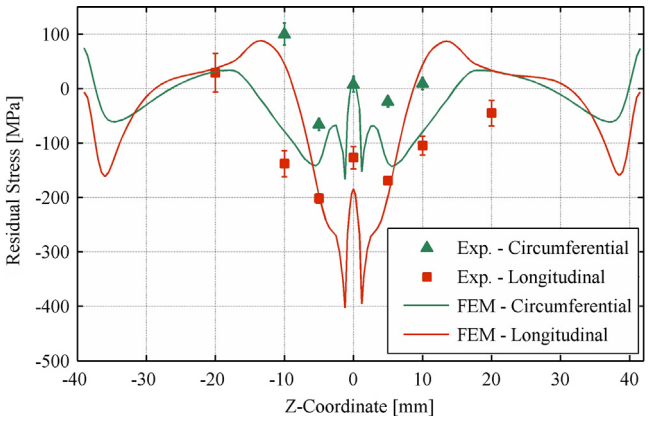

Fig. 16. Comparison of residual stress distribution obtained experimentally with those from FE simulation.

imply that the heat losses during experiments would be a little different from those predicted by the simulation.

X-ray diffraction technique was employed for measuring the residual stresses on the external surface. It may be mentioned that in this technique, the estimated strains which are measured by the shift in the position of diffraction peak are then converted into stresses. The details pertaining to the determination of residual stresses using X-ray diffraction technique are given elsewhere [26,27]. Since the FE simulation did not reveal any remarkable variation of radial stresses, the longitudinal and circumferential stresses only are considered. The longitudinal stresses were measured at seven different locations, viz. at WC and at 5, 10 and 20 mm away from the WC on the both sides of the weld. The locations for the circumferential stresses were at the WC, and at 5 and 10 mm away from the WC on the both sides of weld. The experimental results along with those from FE simulation are plotted in Fig. 16 with error bars for the experimental data. It could be seen that in addition to the close match of trend, the results are in reasonable agreement with each other. The experimental validation of FE results typically obtained for the case of weld speed = 1 mm/s and power = 300 W (i.e. heat input = 300 J/mm) signifies that the computational procedure followed in this investigation can be used for studying the distribution of temperature and residual stresses in a GTAW welded single plane circumferential butt joint.

5. Conclusions

The influence of heat source parameters on the temperature and the residual stress distribution for a GTAW circumferential butt joint of AISI 304 stainless steel was studied through FE simulation and the major conclusions drawn are given below.

(a) The analysis of heat source fitting revealed that the heat input of 300 J/mm results in a proper weld penetration and HAZ. For this heat input, a considerable increase in temperature distribution was observed with the increase in the weld speed and power.
(b) The FE analysis of longitudinal and circumferential stresses performed on the inner and outer surfaces as well as along the radial direction revealed a considerable increase with weld speed and power. For the case of 3 mm location away from the WC, the increase in tensile stress was found to be 150 MPa on the inner surface, whereas the increase in compressive stress was 100 MPa on the outer surface. The transition from tensile to compressive and vice versa was found to occur at 1.25 mm depth (i.e. at the mid section) through wall thickness from the outer surface.
(c) The circumferential residual stress distribution also exhibited similar trend with the magnitude of increase in tensile stresses as 120 MPa on the inner surface, while it was 100 MPa for compressive stresses on the outer surface. The transition from tensile to compressive and vice versa occurred at the radial distance from the outer surface which was found to be between 0.5 and 1.0 mm.
(d) The results of the FE simulation revealed that the radial residual stresses were found to be negligible and were not influenced by the variation in the weld speed and power.
(e) The results of longitudinal and circumferential stresses from FE simulation were compared with those obtained experimentally for a typical condition of weld speed = 1 mm/s and power = 300 W (i.e. heat input = 300 J/mm) and revealed reasonable agreement with each other.

Acknowledgments

The authors gratefully acknowledge Mr. S. Mahadevan, Metallurgy and Materials Group (MMG), Indira Gandhi Centre for Atomic Research (IGCAR) for his valuable support during experimental measurement of residual stress and Dr. C. Phaniraj and Dr. S. Murugan, MMG, IGCAR for fruitful discussions. We also sincerely thank Dr. Baldev Raj, former Director, IGCAR for his constant encouragement.

References

[1] Murugan S, Rai SK, Kumar PV, Jayakumar T, Baldev Raj Bose MSC. Temperature distribution and residual stresses due to multipass welding in type 304 stainless steel and low carbon steel weld pads. Inter J Press Ves Piping 2001;78:307–17.
[2] Malik AM, Qureshi EM, Dar NU, Khan I. Analysis of circumferentially arc welded thin-walled cylinders to investigate the residual stress fields. Thin-Walled Struct 2008;46(12):1391–401.
[3] Lee C-H, Chang K-H. Three-dimensional finite element simulation of residual stresses in circumferential welds of steel pipe including pipe diameter effects. Mater Sci Eng A 2008;487(1–2):210–8.
[4] Shim Y, Feng Z, Lee S, Kim D, Jaeger J, Papritan JC, et al. Determination of residual stresses in thick-section weldments. Weld J 1992;71(9):305s–12s.
[5] Wang L, Felicelli SD, Pratt P. Residual stresses in LENS-deposited AISI 410 stainless steel plates. Mater Sci Eng A 2008;496(1–2):234–41.
[6] Spina R, Tricarico L, Basile G, Sibillano T. Thermo-mechanical modeling of laser welding of AA5083 sheets. J Mater Process Technol 2007;191:215–9.
[7] Brickstad B, Josefsonb BL. A parametric study of residual stresses in multi-pass butt-welded stainless steel pipes. Inter J Press Ves Piping 1998;75:11–25.
[8] Ogawa K, Deng D, Kiyoshima S, Yanagida N, Saito K. Investigations on welding residual stresses in penetration nozzles by means of 3D thermal elastic plastic FEM and experiment. Comp Mater Sci 2009;45:1031–42.
[9] Li C, Wang Y, Zhan H, Han T, Han B, Zhao W. Three-dimensional finite element analysis of temperatures and stresses in wide-band laser surface melting processing. Mater Design 2010;31:3366–73.
[10] Kermanpur M, Shamanian V, Yeganeh E. Three-dimensional thermal simulation and experimental investigation of GTAW circumferentially butt-welded Incoloy 800 pipes. J Mater Process Technol 2008;199:295–303.
[11] Wu CS, Sun JS. Numerical analysis of temperature field during double-sided arc welding of thick materials. Comp Mater Sci 2002;25:457–68.
[12] Wu CS, Wang HL, Zhang YM. Numerical analysis of the temperature profiles and weld dimension in high power direct-diode laser welding. Comp Mater Sci 2009;46:49–56.
[13] Gery D, Long H, Maropoulos P. Effects of welding speed, energy input and heat source distribution on temperature variations in butt joint welding. J Mater Process Technol 2005;167:393–401.
[14] Deng D, Kiyoshima S. Numerical simulation of welding temperature field, residual stress and deformation induced by electro slag welding. Comp Mater Sci 2012;62:23–34.
[15] Deng D. FEM prediction of welding residual stress and distortion in carbon steel considering phase transformation effects. Mater Des 2009;30:359–66.
[16] Farid V-T, Ali Z-A. Numerical and experimental investigation of T-shape fillet welding of AISI 304 stainless steel plates. Mater Des 2013;47:615–23.
[17] Long H, Gery D, Carlier A, Maropoulos PG. Prediction of welding distortion in butt joint of thin plates. Mater Des 2009;30:4126–35.
[18] del Coz Díaz JJ, Menéndez Rodríguez P, García Nieto PJ, Castro-Fresno. D. Comparative analysis of TIG welding distortions between austenitic and duplex stainless steel s by FEM. Appl Therm Eng 2010;30:2448–59.
[19] Jiang WC, Wang BY, Gong JM, Tu ST. Finite element analysis of the effect of welding heat input and layer number on residual stress in repair welds for a stainless steel clad plate. Mater Des 2011;32:2851–7.

[20] Tian Y, Wang C, Zhu D, Zhou Y. Finite element modeling of electron beam welding of a large complex Al alloy structure by parallel computations. J Mater Process Technol 2008;199:41–8.
[21] Sysweld reference manual and material data, ESI group; 2005.
[22] Goldak JA, et al. Coupling heat transfer, microstructure evaluation and thermal stress analysis in weld mechanics. In: Karlsson L, et al., editors. Mechanical effect of welding, IUTAM symposium. Springer Berlin Heidelberg: Springer-Verlag; 1992. p. 1–30.
[23] Zain-ul-abdein M, Nélias D, Jullien J-F, Boitout F, Dischert L, Noe X. Finite element analysis of metallurgical phase transformations in AA 6056-T4 and their effects upon the residual stress and distortion states of a laser welded T-joint. Inter J Press Ves Piping 2011;88:45–56.
[24] Dean D, Hidekazu M. Numerical simulation of temperature field and residual stress in multi-pass welds in stainless steel pipe and comparison with experimental measurements. Comp Mater Sci 2006;37(3):269–77.
[25] Dean D, Hidekazu M, Wei L. Numerical and experimental investigations on welding residual stress in multi-pass butt-welded austenitic stainless steel pipe. Comp Mater Sci 2008;42(2):234–44.
[26] Norton JT. X-ray determination of residual stress. Mater Eval 1973, February;31:21A.
[27] Noyan IC, Cohen JB. Residual stress-measurement by diffraction and interpretation. In: IIschner B, Grant NJ, editors. A very complete treatment of stress and stress tensors and how stresses are measured in polycrystalline samples. New York: Springer-Verlag; 1987.